ACS Photonics

pubs.acs.org/journal/apchd5

Article

Reconfigurable Surface Plasmon Resonance Photodetector with a MEMS Deformable Cantilever

Masaaki Oshita, Hidetoshi Takahashi, Yoshiharu Ajiki, and Tetsuo Kan*

Cite This: https://dx.doi.org/10.1021/acsphotonics.9b01510

Read Online

ACCESS | Metrics & More | Article Recommendations

ABSTRACT: Plasmonic photodetectors have many useful characteristics, such as wavelength- or polarization-specific photodetection. Although reconfigurable plasmonic structures have been intensively studied, reconfiguration of the optical characteristics of a plasmonic photodetector has not yet been reported. Here, we report a gold diffraction-grating-type plasmonic photodetector that reconfigures its optical characteristics with a MEMS deformable cantilever. By reconfiguring the photodetector characteristics using an angular scan of the cantilever over −21° to 21°, the peak shifts of the photocurrent signal waveform are found to depend on the wavelength over 1200∼1500 nm, which is consistent with SPR theory. The proposed reconfigurable plasmonic photodetector allowed us to obtain spectroscopic information on the light in a demonstration experiment.

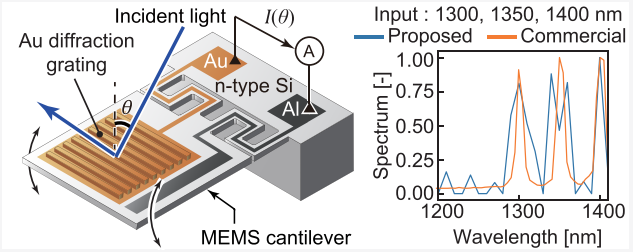

KEYWORDS: *photodetector, MEMS, surface plasmon resonance, Schottky-barrier, near-infrared light, spectrometer*

Plasmonic photodetectors have been intensively studied[1−3] because they offer many useful characteristics, such as improvement of photodetection sensitivity,[4,5] wavelength- or polarization-specific photodetection,[6−8] and infrared light detection with silicon.[9] Since the plasmonic structures are usually very thin (as thin as 100 nm), it is not necessary to sacrifice the compactness of the photodetector to add these functions. In this paper, we report on a photodetector equipped with gold grating structures on a tilting-angle micro-electromechanical system (MEMS) cantilever to reconfigure plasmonic photodetection characteristics and experimentally demonstrated spectroscopic measurement using the reconfigurable plasmonic photodetector. Reconfigurable plasmonic structures themselves have been widely studied,[10−13] and dynamic reconfiguration, such as deformation of device structures[13−23] or application of bias voltage,[24,25] provides a unique and fascinating functionality compared with static structures: active control of color of the reflected light, alternation of the spectrum or focal length of the transmitted light, phase shift control of the transmitted light, and so on.[13−25] Despite many studies on such reconfigurable plasmonics, studies on a reconfigurable plasmonic photodetector have not yet been reported; if dynamic tuning of detectable wavelengths or polarizations becomes possible, emerging new application fields can be expected, such as spectroscopy and polarimetry.

PRINCIPLE OF THE PHOTODETECTOR

Here, we report on a MEMS reconfigurable plasmonic photodetector. A MEMS angular scanning mechanism is equipped with a plasmonic gold diffraction grating fabricated on an n-type silicon (n-Si) cantilever (Figure 1a). When transverse magnetic (TM)-polarized near-infrared light is incident on the grating with a certain angle of incidence θ, surface plasmon resonance (SPR) is generated on the grating when the SPR matching conditions, namely, the angle of incidence and wavelength, are satisfied. The incident light is then absorbed on the grating surface as SPR, and the absorbed light excites free electrons in the gold layer. Since a Schottky barrier is formed on an interface between the gold and the n-Si, these electrons overcome the Schottky barrier so that the SPR can be electrically transduced to a photocurrent $I(\theta)$, enabling SPR-based photodetection. In addition, since the cantilever is deflectable, reconfiguration of the SPR matching condition and photodetection characteristics can be performed by tilting the cantilever to change the incident angle of light θ by an external actuation force. Two zigzag cantilever feet are used to decrease the stiffness and increase the amplitude of the change in the incident angle.[26] In one example and this time, acoustic pressure was applied from the backside of the grating to tilt the cantilever.[27] A large tilting angle can be obtained by tuning the acoustic wave frequency to be identical to the mechanical resonant frequency of the cantilever. The incident angle to the

Received: October 16, 2019
Published: February 4, 2020

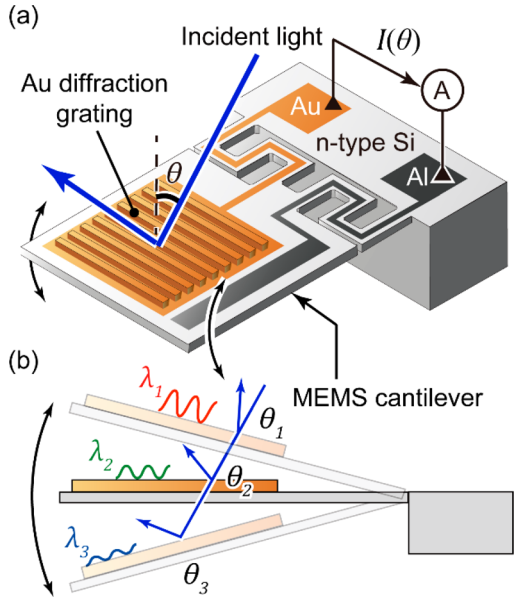

Figure 1. Schematic of the MEMS cantilever with a gold diffraction grating.

grating is then scanned. The scanning range could be, for example, from θ_1 through θ_2 to θ_3, as in Figure 1b, corresponding to the scanning of SPR matching conditions. As described in this paper, we designed and fabricated devices and evaluated their electrical characteristics. The reconfiguration performance of the SPR photodetector was evaluated by measuring the photocurrent for monochromatic laser light with various wavelengths incident on the grating during the cantilever tilting.

SIMULATION AND FABRICATION

The structure and dimensions of the device and the grating are shown in Figure 2a,b. The device was fabricated using a silicon on insulator (SOI) wafer; the thicknesses of the device layer, buried oxide layer and handle layer were 25, 1.5, and 500 μm, respectively. The cantilever incorporates a grating formed on a square plate supported by two zigzag feet. A gold grating was formed at the center of the square plate, which acted as an SPR coupling site. The gold layer also served as an anode electrode. The size of the plate was a square with a side length of 2500 μm, and the grating area size was a square with a side length of 1850 μm. The aluminum electrode was patterned in addition to the grating to fabricate the cathode electrode on the n-Si surface. The zigzag feet decrease the stiffness of the cantilever, decreasing the mechanical resonant frequency and increasing the alteration amplitude of the incident angle. Each foot had six 90° turns, and each turn component was 125 μm in width and 937 μm in length. These structural parameters were chosen such that the cantilever had a primary resonant frequency within the audible range, which was easy to activate with a speaker. The resonant frequency of these structural parameters was calculated using commercially available finite element method software (COMSOL Multiphysics ver. 5.4, COMSOL, U.S.A.), and the primary and secondary resonant frequencies were calculated to be 391 and 1681 Hz, respectively (Figure 2c,d). Since in the primary mode the cantilever presents a deformation that offers only θ tilting, this mode was employed in the latter experiments. On the zigzag feet, Au and Al wirings were patterned, and electrical pads of

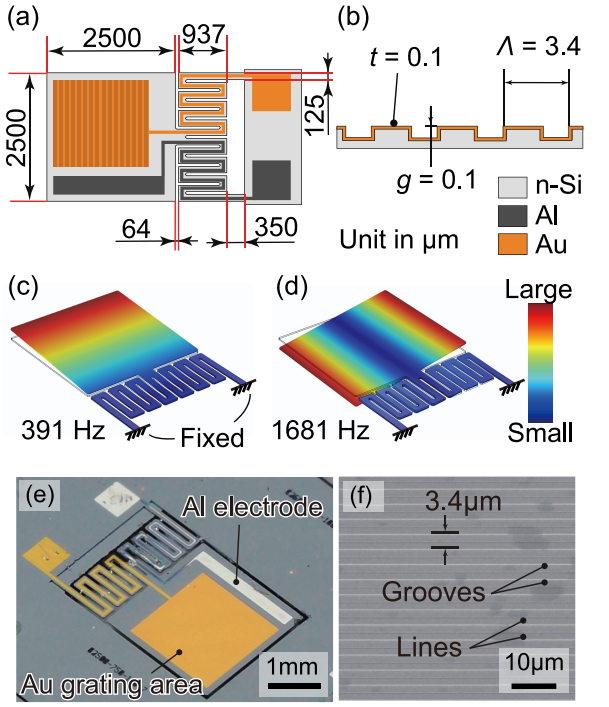

Figure 2. Device design overview, (a) dimensions of the cantilever, (b) dimensions of the grating, (c, d) results of FEM simulations of the cantilever mechanical deformation at the primary and secondary mechanical resonant frequencies, (e) a photograph of the device, and (f) an SEM micrograph of the grating.

Au and Al were formed around the root of the feet. The dimensions of the gold diffraction grating essentially followed those in ref 28. The grating pitch Λ was 3.4 μm, and the groove height g was 100 nm (Figure 2b). The grating grooves were formed on the device layer of the SOI wafer by reactive ion etching. The Au layer with a thickness t of 100 nm was deposited obliquely at 20° with rotation to cover the entire surface of the grating. An Al layer was also deposited as a cathode electrode. The device layer and the handle layer were then removed by deep reactive ion etching. The cantilever was ultimately released by removing the buried oxide layer with vapor HF etching. A photograph and micrograph of the fabricated device are shown in Figure 2e and f, respectively.

CHARACTERISTIC OF THE PHOTODETECTOR

The Schottky barrier height of the fabricated device was calculated from the IV characteristics of the device based on the method in ref 29. The calculated value was 0.79 eV, where the temperature of the device was 293 K, and the effective area of the diode was 0.068 cm^2. Since the cutoff wavelength calculated from the Schottky barrier height was approximately 1.57 μm, the fabricated device had the ability to detect near-infrared light. The SPR generation and detection ability of the fabricated device was investigated. The SPR coupling angles are theoretically calculated by using the equation below.[30,31]

$$\theta = \sin^{-1}\frac{1}{\sqrt{\epsilon_{air}}}\left\{\mathrm{Re}\left(\sqrt{\frac{\epsilon_{air}\epsilon_{Au}}{\epsilon_{air}+\epsilon_{Au}}}\right) - m\frac{2\pi}{\Lambda k_0}\right\} \quad (1)$$

where θ is the angle of incidence where SPR is induced, k_0 is the wavenumber of the light in vacuum, Λ is the pitch of the Au grating, m is the diffraction order, ϵ_{air} is the relative

https://dx.doi.org/10.1021/acsphotonics.9b01510
ACS Photonics XXXX, XXX, XXX−XXX

permittivity of air, and ϵ_{Au} is the relative permittivity of Au. Since the SPR coupling angle θ is thus dependent on the wavelength of the incident light, we investigated the SPR behavior by changing the wavelength of the incident light without dynamic tilting of the cantilever. The device was attached to a rotation stage such that the groove of the grating was parallel to the axis of rotation (Figure 3a). Monochromatic

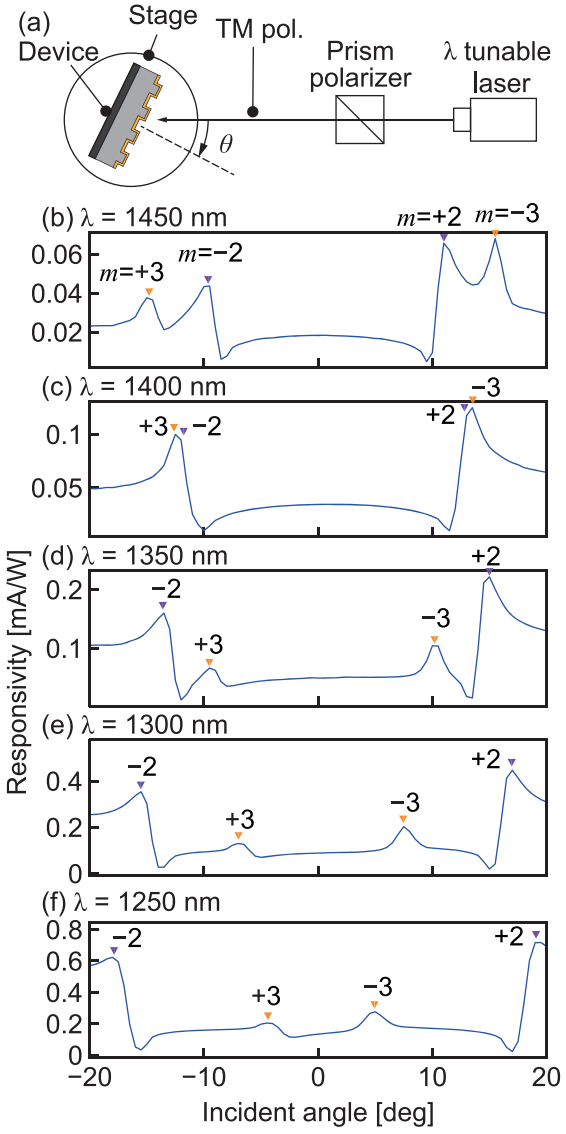

Figure 3. (a) An experimental setup to rotate the device and measure the photocurrent; (b)−(f) obtained photocurrent angular spectra for wavelengths 1450, 1400, 1350, 1300, and 1250 nm.

near-infrared light from the light source (SC450−2, FIANIUM, U.K.) was converted into TM polarized light by transmission through a polarizer. The wavelength of this light ranged from 1200 to 1500 nm. The photocurrent signal from the electrode of the device was measured by scanning the angle of incidence θ of the rotation stage: −20° to 20°. The photocurrent from the device was converted into voltage by an op-amp and measured by a DC voltage current monitor (6242, ADCMT, Japan). Both the MEMS device and the electrical circuit were embedded in a shield box to eliminate ambient noise. The cantilever was positioned behind an aperture in the shield box surface such that the light fell on the grating of the device. photocurrent signals for five different wavelengths are shown in Figure 3b−f. The photocurrent signals were expressed as responsivity which is defined by the photocurrent divided by the input intensity of each wavelength measured by a power meter (PM320E-S122C, Thorlabs, U.S.A.). Distinctive peaks appeared on the photocurrent signals, and the corresponding diffraction orders m were also shown. Since these peak angular positions systematically shifted as the wavelength changed, they can be attributed to SPR. For further verification, the experimental and theoretical relations of the wavelength and the angle of incidence at the peak of the photocurrent signal are plotted in Figure 4; the experimental

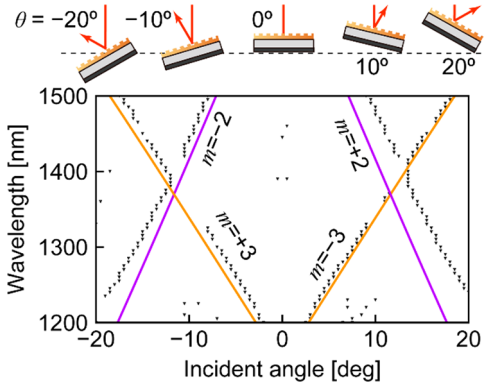

Figure 4. Dispersion relation between the angle of incidence and the SPR coupling wavelength. Dots indicate experimental values, and the solid lines are theoretical predictions.

data were extracted from the previous experiments. In the calculation, the permittivity of Au was obtained from.[32] The numbers in the graph plot indicate the corresponding diffraction orders m for each peak. Since the experimental and theoretical results are clearly consistent, we concluded that the fabricated device was able to detect SPR electrically on its gold diffraction grating.

ESTIMATION OF THE TILTING ANGLE AMPLITUDE OF THE CANTILEVER

We then investigated whether the fabricated device could produce an adequate angle tilting amplitude, comparable to that of a previous experiment with a rotation stage. The resonant frequency of the cantilever deflection was first measured using a laser Doppler vibrometer (MLD-221D, Neoarc Corp., Japan). The device chip was mounted on a PZT actuator such that an external vibration in the out-of-plane direction could be applied. The laser spot was focused on one end of the cantilever beam to measure the vibrational velocity of the beam for frequencies from 20 to 2000 Hz, and the gain plot of the amplitude relative to the rigid substrate around the cantilever was obtained as shown in Figure 5a. The primary resonance appeared at 395 Hz, which is highly consistent with the FEM result and indicates that the zigzag feet of the cantilever worked effectively to decrease the resonant frequency. The amplitude of the tilting angle in an actual SPR modulation environment was measured using the experiment system shown in Figure 5b. The grating on the device was irradiated with a visible light laser through a hole on a screen in front of the device. Cantilever tilting was produced by sound pressure from a speaker (FF125 K, FW208N, FOSTEX, Japan) behind the device. When the cantilever tilted,

https://dx.doi.org/10.1021/acsphotonics.9b01510
ACS Photonics XXXX, XXX, XXX−XXX

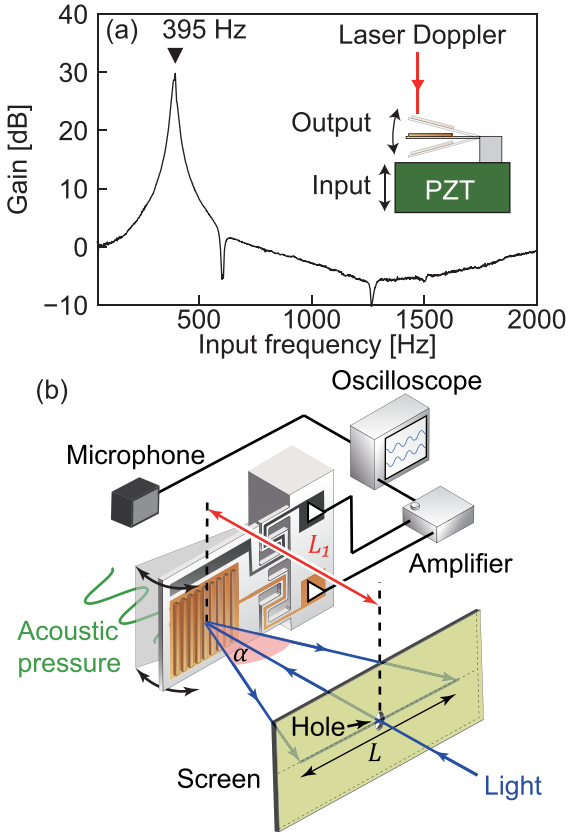

Figure 5. Mechanical resonant characteristics of the cantilever: (a) a deflection amplitude gain plot relative to the substrate using laser Doppler velocimetry and (b) an experimental setup for measuring the scan angle by measuring the line length L on a screen drawn by a reflected laser light spot.

the reflected beam, which is the zeroth diffraction, draws a line with a length of L on the screen, which is located at a distance L_1 from the cantilever. The tilting angle amplitude α was derived by eq 2 below.

$$\alpha = 2\tan^{-1}\frac{1}{2}\frac{L}{L_1} \tag{2}$$

The sound pressure applied on the cantilever was simultaneously measured by a microphone (MB-2200M10, Ono Sokki, Japan) next to the cantilever, and the sound pressure was verified to record the harmonic waveform. We then investigated whether the mechanical resonant frequency was consistent with the previous vibrometer measurement and COMSOL analysis. The resonance frequency of the cantilever f_c was determined by finding the maximum L during the sweeping frequency of the sound from a speaker; $f_c \sim 374$ Hz, consistent with both the FEM and the laser Doppler experiment results. Since the measured L and L_1 were respectively 230 and 127 mm at the resonant frequency with a sound pressure amplitude of 28.8 Pa, the tilting amplitude α was calculated to be 84.0°. Assuming that vibration of the cantilever was symmetric between deflections in the forward and backward directions, the tilting angle amplitude $\alpha = 84.0°$ corresponds to the incident angle, which ranged from −21.0° to 21.0°, almost equivalent to the results of the previous rotation stage experiment: the angle of incidence ranging from −20° to 20°. We therefore concluded that the device had the ability to obtain an adequate tilting angle amplitude for SPR measurements.

DYNAMICS SPR PHOTOCURRENT DETECTION DURING THE VIBRATION OF THE CANTILEVER BY ACOUSTIC PRESSURE

We investigated whether the fabricated device could reconfigure the SPR coupling condition and perform electrical photodetection via SPR. The signal of the sound pressure from the microphone and the photocurrent signal from the device were recorded on the oscilloscope (TBS 1052B-EDU, Tektronix, U.S.A.) at the same time as shown in Figure 5b. Monochromatic near-infrared light was incident into the grating under the same conditions as in the previous experiment, and photocurrent signals were measured during the cantilever tilting. Since the cantilever oscillates driven by the application of sinusoidal sound pressure, the photocurrent waveform also repeats a single cycle waveform. Single cycle waveforms for different wavelengths incidence were extracted to be compared with data in Figures 3b–f and 6; the cantilever deflection at each position of the single cycle is shown in Figure 6a, and the photocurrent waveforms for different wavelengths are shown in Figure 6b–f. Note that the cantilever did not have a displacement sensor inside, and the cycle period was determined using the sound pressure measured by a microphone near the cantilever. The phase position among the

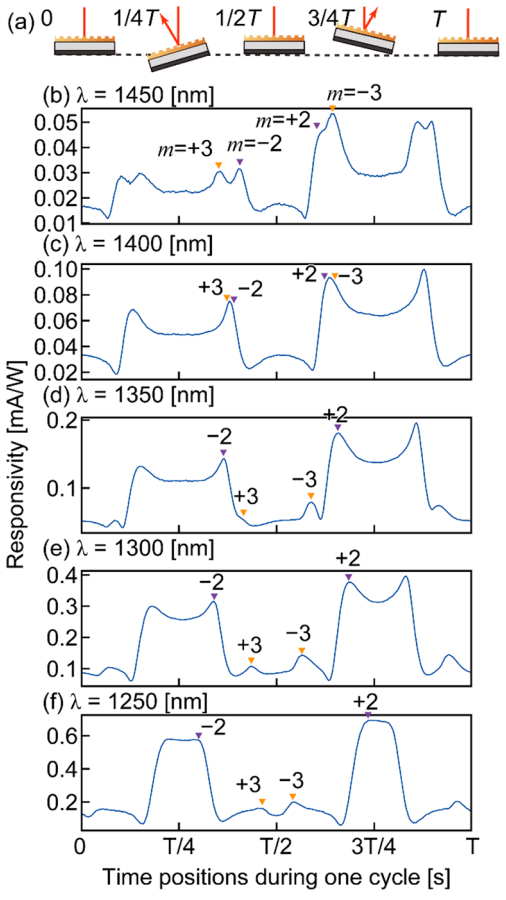

Figure 6. Dynamic deflection and reconfiguration of SPR coupling conditions: (a) relationship between the time position during one cycle T and the cantilever deflection status and (b)–(f) obtained photocurrents for five different input wavelengths.

https://dx.doi.org/10.1021/acsphotonics.9b01510
ACS Photonics XXXX, XXX, XXX−XXX

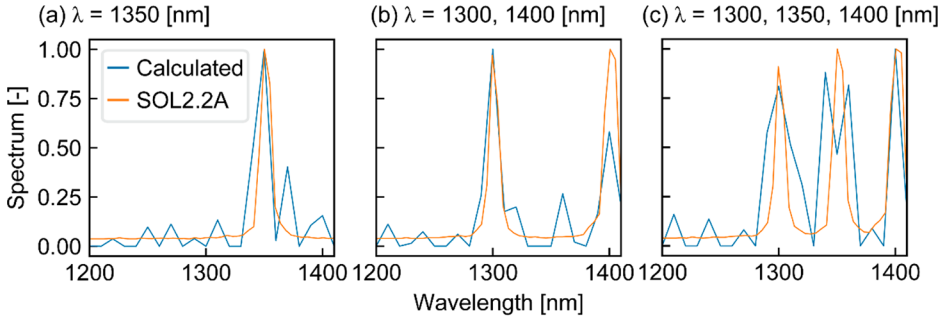

Figure 7. Spectra obtained from a photocurrent for one or more input wavelengths (a) 1350 nm, (b) 1300 and 1400 nm, and (c) 1300, 1350, and 1400 nm. These spectra were compared with a spectrum obtained from a commercial near-infrared spectrometer (SOL2.2A, BWTEK, U.S.A.).

cycle period should be determined to investigate the photocurrent waveform. Since the SPR signal for λ = 1250 nm in Figure 3 presents peaks around the incident angle 20°, the phase timings of a cycle of the photocurrent signal for all wavelengths were determined such that the peak for λ = 1250 nm among a waveform situated at $T/2$ and $3T/4$ of each cycle period, where $T = 1/f_c$. Since the cantilever experiences a certain incident angle two times for each resonant cycle round trip, the waveform in Figure 6 virtually contained two cycle periods of the waveform of Figure 3. Since the amplitude of sound pressure applied on the cantilever was almost equal to that in the previous experiment, the scan angle range in this experiment was almost the same. Therefore, the range of the phase from $T/4$ to $3T/4$ corresponded to the range of incident angles from −21° to 21°. A comparison between the results on a rotation stage in Figure 3 and those in Figure 6 shows that the signal for the sound pressure actuation is slightly distorted. However, there are still distinctive peaks on the waveform indicated by diffraction orders m and a similarity to the SPR waveform using a rotation stage. For example, the lateral distance between peaks corresponding to m = −3 and +3 near $T/2$ increases with increasing wavelength. This behavior is consistent with the theoretical and experimental dispersion relation, as shown in Figure 3. In addition, the lateral distances between m = +3 and −2 or between m = −3 and +2 peaks decreased with increasing wavelength, although m = ±2 peaks are not observable for λ = 1400 nm. These tendencies are also consistent with theory and previous experiments. The waveform distortion might originate from transient phenomena, which can be attributed to the response time of the peripheral circuit and an inductance or a capacitance factor among the device. Among them, a long time constant of the current−voltage transimpedance amplifier in a peripheral circuit can be a major factor because an amplification resistor as large as 10 MΩ was used to amplify the current. These problems can be, however, eliminated by optimizing the peripheral circuit or the plasmonic structure on the cantilever, as in the strategy used in ref 33, where the sharper plasmonic response was obtained using higher diffraction orders to couple SPR. We therefore conclude that the fabricated device can perform a reconfiguration of the SPR resonant condition on a small MEMS chip and detect SPR electrically to provide plasmonic photodetection at the same time.

DEMONSTRATION OF SPECTROSCOPY USING RECONFIGURABILITY

Finally, we demonstrated spectroscopic measurement by making use of reconfigurability of the proposed device. Spectroscopy methods using angular dependent photocurrent from plasmonic photodetector equipped with gratings have already been achieved in refs 28 and 34, where no reconfigurable MEMS had not been applied yet. This method utilizes the fact that the SPR angle on the grating differs depending on the wavelength of the incident light. The method retrieves the spectrum of the light from the angular photocurrent spectrum measured during scanning the angle of incident of the light on the device. We then applied this method to the proposed device and demonstrated spectroscopy function; that is, the light was incident on the photodetector during acoustic vibration, and the spectrum of the light was retrieved from the photocurrent waveform data. It is noted that time positions during one cycle of the cantilever vibration were employed instead of angle of incidence in this retrieval procedure, unlike previous work in refs 28 and 34. The same experimental system with the one in Figure 5b was used. Since in the spectrum retrieval the photodetector response for each monochromatic light should be obtained as a characteristic data beforehand, measurement data of the previous experiments using acoustic pressure (Figure 6) were used here. Photocurrents were then measured for the light, which contained several monochromatic light components with different wavelengths from each other entered onto the device simultaneously, and the spectrum for these light inputs was retrieved. Combinations of input wavelengths were three patterns: (a) single wavelength λ = 1350 [nm], (b) two wavelengths λ = 1300 and 1400 nm, (c) three wavelengths λ = 1300, 1350, and 1400 nm. In addition, incident light spectra were also measured by a commercial near-infrared spectrometer (SOL2.2A, BWTEK, U.S.A.). Each spectrum obtained from the method and the commercial spectrometer are shown in Figure 7. The blue lines represent a spectrum obtained with the method, and the orange lines represent a spectrum obtained with the commercial spectrometer. Since the retrieved spectra were consistent with the ones obtained with a commercial spectroscopy regarding the peak wavelength positions, it can be concluded that the spectrum retrieval using the proposed device could be performed. The retrieved spectrum shapes are, however, not smooth and have some artifacts, and wavelength resolution is still limited. These smoothness and artifact problems will be able to be solved by improvement of the device performances such as sensitivity of the photodetector. In addition, since the wavelength resolution is mainly determined by the sharpness of SPR waveform, optimization of resonant grating structure will improve the resolution. Since this spectroscopy measurement is realized by taking advantage of the proposed device, it can be concluded

https://dx.doi.org/10.1021/acsphotonics.9b01510
ACS Photonics XXXX, XXX, XXX−XXX

that the demonstration presents availability of the reconfigurable plasmonic photodetector.

CONCLUSION AND OUTLOOK

In this paper, we proposed a reconfigurable SPR photodetector by integrating a plasmonic grating Si photodetector and a MEMS cantilever structure. Since the feet of the MEMS cantilever were configured as zigzags, the amplitude of alteration of an incident angle was enhanced to effectively reconfigure SPR coupling conditions. SPR generated on the gold diffraction grating is detected as a photocurrent signal. It was verified that the fabricated device could induce SPR on the device, consistent with theory. The alternation of the incident angle by the cantilever deflection successfully reconfigured the SPR coupling condition. The performance of the reconfiguration was confirmed by irradiation with monochromatic light at wavelengths of 1200 to 1500 nm with an interval of 5 nm during mechanical resonant deflection of the cantilever. This reconfiguration provided angular SPR-induced photocurrent waveforms, and it was possible to confirm the peak shifts of the photocurrent signal depending on an incident wavelength, which is consistent with SPR theory. Finally, we demonstrated spectroscopic measurement using the reconfigurability of the proposed device. Spectra obtained from the proposed device were consistent with the ones measured with a commercial spectrometer. We therefore conclude that the proposed device achieved SPR coupling reconfiguration of the plasmonic photodetector. In addition, the proposed structure senses only TM-polarized light, so the polarization-specific measurement of the incident light is also possible. For example, by making the deflection direction orthogonal to that of the current device, the transverse electric (TE) polarization can also be measured. This functionality will enable spectroscopy with information on the polarization states of the incident light with a one-chip device. Reconfiguration of the plasmonic photodetector provides many fascinating applications, and the results demonstrated here make an important contribution toward new plasmonic devices.

AUTHOR INFORMATION

Corresponding Author

Tetsuo Kan − *Department of Mechanical Engineering and Intelligent Systems, Graduate School of Informatics and Engineering, The University of Electro-Communications, Tokyo 182-8585, Japan;* orcid.org/0000-0002-1433-9465; Email: tetsuokan@uec.ac.jp

Authors

Masaaki Oshita − *Department of Mechanical Engineering and Intelligent Systems, Graduate School of Informatics and Engineering, The University of Electro-Communications, Tokyo 182-8585, Japan*

Hidetoshi Takahashi − *Department of Mechanical Engineering, Faculty of Science and Technology, Keio University, Yokohama-city, Kanagawa 223-8522, Japan*

Yoshiharu Ajiki − *Department of Mechanical Engineering and Intelligent Systems, Graduate School of Informatics and Engineering, The University of Electro-Communications, Tokyo 182-8585, Japan; Microtechnology R&D Division, Olympus Corporation, 192-8512 Tokyo, Japan*

Complete contact information is available at: https://pubs.acs.org/10.1021/acsphotonics.9b01510

Author Contributions

M.O. fabricated the photodetector, developed the optical measurement systems, acquired and analyzed the data, and wrote the manuscript. H.T. proposed the zigzag feet of the cantilever and measured the vibration characteristics of the cantilever. Y.A. contributed to the analysis of the Schottky-barrier responses. T.K. supervised the project, performed data analysis, and wrote the manuscript. All authors contributed to the discussion of the results.

Funding

This research was financially supported by Aisin Cosmos R&D Co., Ltd. and partly funded by the TATEISHI Science and Technology Foundation.

Notes

The authors declare no competing financial interest.

ACKNOWLEDGMENTS

The photolithography masks were made using the University of Tokyo VLSI Design and Education Center (VDEC)'s 8-in. EB writer F5112 + VD01 donated by ADVANTEST Corporation. Dr. Tsukagoshi provided helpful support for MEMS fabrication. Microfabrication was performed in a clean room of the Division of Advanced Research Facilities (DARF) of the Coordinated Center for UEC Research Facilities of the University of Electro-Communications, Tokyo, Japan.

REFERENCES

(1) Schuller, J. A.; Barnard, E. S.; Cai, W.; Jun, Y. C.; White, J. S.; Brongersma, M. L. Plasmonics for extreme light concentration and manipulation. *Nat. Mater.* **2010**, *9* (3), 193−204.

(2) Brongersma, M. L. Plasmonic Photodetectors, Photovoltaics, and Hot-Electron Devices. *Proc. IEEE* **2016**, *104* (12), 2349−2361.

(3) Dorodnyy, A.; et al. Plasmonic Photodetectors. *IEEE J. Sel. Top. Quantum Electron.* **2018**, *24* (6), 1−13.

(4) Ogawa, S.; Okada, K.; Fukushima, N.; Kimata, M. Wavelength selective uncooled infrared sensor by plasmonics. *Appl. Phys. Lett.* **2012**, *100* (2), 021111.

(5) Hui, Y.; Gomez-Diaz, J. S.; Qian, Z.; Alù, A.; Rinaldi, M. Plasmonic piezoelectric nanomechanical resonator for spectrally selective infrared sensing. *Nat. Commun.* **2016**, *7*, 1−9.

(6) Jestl, M.; Kock, A.; Beinstingl, W.; Gornik, E. Polarization- and wavelength-selective photodetectors. *J. Opt. Soc. Am. A* **1988**, *5* (9), 1581−1584.

(7) Sobhani, A.; Knight, M. W.; Wang, Y.; Zheng, B.; King, N. S.; Brown, L. V.; Fang, Z.; Nordlander, P.; Halas, N. J. Narrowband photodetection in the near-infrared with a plasmon-induced hot electron device. *Nat. Commun.* **2013**, *4*, 1643−1646.

(8) Chalabi, H.; Schoen, D.; Brongersma, M. L. Hot-electron photodetection with a plasmonic nanostripe antenna. *Nano Lett.* **2014**, *14* (3), 1374−1380.

(9) Ajiki, Y.; Kan, T.; Yahiro, M.; Hamada, A.; Adachi, J.; Adachi, C.; Matsumoto, K.; Shimoyama, I. Silicon based near infrared photodetector using self-assembled organic crystalline nanopillars. *Appl. Phys. Lett.* **2016**, *108* (15), 151102.

(10) Degl'Innocenti, R.; Kindness, S. J.; Beere, H. E.; Ritchie, D. A. All-integrated terahertz modulators. *Nanophotonics* **2018**, *7* (1), 127−144.

(11) Bang, S.; Kim, J.; Yoon, G.; Tanaka, T.; Rho, J. Recent advances in tunable and reconfigurable metamaterials. *Micromachines* **2018**, *9* (11), 560.

(12) Midolo, L.; Schliesser, A.; Fiore, A. Nano-opto-electro-mechanical systems. *Nat. Nanotechnol.* **2018**, *13* (1), 11−18.

(13) Xiong, K.; Tordera, D.; Jonsson, M. P.; Dahlin, A. B. Active control of plasmonic colors: Emerging display technologies. *Rep. Prog. Phys.* **2019**, *82* (2), 024501.

(14) Tao, H.; Strikwerda, A. C.; Fan, K.; Padilla, W. J.; Zhang, X.; Averitt, R. D. Reconfigurable terahertz metamaterials. *Phys. Rev. Lett.* **2009**, *103* (14), 1−4.
(15) Holsteen, A. L.; Cihan, A. F.; Brongersma, M. L. Temporal color mixing and dynamic beam shaping with silicon metasurfaces. *Science* **2019**, *365*, 257−260.
(16) Lapine, M.; Shadrivov, I. V.; Powell, D. A.; Kivshar, Y. S. Magnetoelastic metamaterials. *Nat. Mater.* **2012**, *11* (1), 30−33.
(17) Thijssen, R.; Verhagen, E.; Kippenberg, T. J.; Polman, A. Plasmon nanomechanical coupling for nanoscale transduction. *Nano Lett.* **2013**, *13* (7), 3293−3297.
(18) Ou, J. Y.; Plum, E.; Zhang, J.; Zheludev, N. I. An electromechanically reconfigurable plasmonic metamaterial operating in the near-infrared. *Nat. Nanotechnol.* **2013**, *8* (4), 252−255.
(19) Dennis, B. S.; Haftel, M. I.; Czaplewski, D. A.; Lopez, D.; Blumberg, G.; Aksyuk, V. A. Compact nanomechanical plasmonic phase modulators. *Nat. Photonics* **2015**, *9* (4), 267−273.
(20) Ee, H. S.; Agarwal, R. Tunable Metasurface and Flat Optical Zoom Lens on a Stretchable Substrate. *Nano Lett.* **2016**, *16* (4), 2818−2823.
(21) Honma, H.; Mitsudome, M.; Ishida, M.; Sawada, K.; Takahashi, K. Nano-optomechanical characterization of surface-plasmon-based tunable filter integrated with comb-drive actuator. *J. Micromech. Microeng.* **2017**, *27* (3), 034001.
(22) Chen, W.; et al. Ultrasensitive, Mechanically Responsive Optical Metasurfaces via Strain Amplification. *ACS Nano* **2018**, *12* (11), 10683−10692.
(23) Roy, T.; Zhang, S.; Jung, I. W.; Troccoli, M.; Capasso, F.; Lopez, D. Dynamic metasurface lens based on MEMS technology. *APL Photonics* **2018**, *3* (2), 021302.
(24) Yao, Y.; et al. Electrically tunable metasurface perfect absorbers for ultrathin mid-infrared optical modulators. *Nano Lett.* **2014**, *14* (11), 6526−6532.
(25) Dong, Z.; Sun, C.; Si, J.; Deng, X. A tunable plasmonic nano-Antenna based on metal-graphene double-nanorods. *Laser Phys. Lett.* **2018**, *15* (5), 056202.
(26) Isozaki, A.; Kan, T.; Takahashi, H.; Matsumoto, K.; Shimoyama, I. Out-of-plane actuation with a sub-micron initial gap for reconfigurable terahertz micro-electro-mechanical systems metamaterials. *Opt. Express* **2015**, *23*, 26243.
(27) Takahashi, H.; Dung, N. M.; Matsumoto, K.; Shimoyama, I. Differential pressure sensor using a piezoresistive cantilever. *J. Micromech. Microeng.* **2012**, *22* (5), 055015.
(28) Chen, W.; Kan, T.; Ajiki, Y.; Matsumoto, K.; Shimoyama, I. NIR spectrometer using a Schottky photodetector enhanced by grating-based SPR. *Opt. Express* **2016**, *24* (22), 25797.
(29) Cheung, S. K.; Cheung, N. W. Extraction of Schottky diode parameters from forward current-voltage characteristics. *Appl. Phys. Lett.* **1986**, *49* (2), 85−87.
(30) Raether, H. *Surface Plasmons on Smooth and Rough Surfaces and on Gratings*; Springer, 1988.
(31) Barnes, W. L.; Dereux, A.; Ebbesen, T. W. Surface plasmon subwavelength optics. *Nature* **2003**, *424* (6950), 824−830.
(32) Rakic, A. D.; Djurisic, A. B.; Elazar, J. M.; Majewski, M. L. Optical properties of metallic films for vertical-cavity optoelectronic devices. *Appl. Opt.* **1998**, *37* (22), 5271−5283.
(33) Cai, D.; Lu, Y.; Lin, K.; Wang, P.; Ming, H. Improving the sensitivity of SPR sensors based on gratings by double-dips method (DDM). *Opt. Express* **2008**, *16* (19), 14597.
(34) Suido, Y.; Yamamoto, Y.; Thomas, G.; Ajiki, Y.; Kan, T. Extension of the Measurable Wavelength Range for a Near-Infrared Spectrometer Using a Plasmonic Au Grating on a Si Substrate. *Micromachines* **2019**, *10* (6), 403.

https://dx.doi.org/10.1021/acsphotonics.9b01510
ACS Photonics XXXX, XXX, XXX−XXX